PROCEEDINGS of the
23rd International Congress on Acoustics

9 to 13 September 2019 in Aachen, Germany

Parallel implementation for three-dimensional acoustic field computation in a penetrable wedge by image source method

Wenbin XIAO [1]; Yongxian WANG [1*]; Wei LIU [1]; Qiang LAN [1]; Xinghua CHENG [1]; Zijie ZHU [1]; Xin WANG [1]; Ben LUO [2], Dezhi WANG [1]; Jiani WU [1], Lilun ZHANG [1]

[1] College of Meteorology and Oceanology, National University of Defense and Technology, P.R.China

[2] School of Traffic & Transportation Engineering, Central South University, P.R.China

ABSTRACT

Present work aims to the parallel implementation of message passing interface (MPI) and open multi-processing (OpenMP) for the three-dimensional acoustic field computation in a penetrable wedge. Possible practical application of the wedge waveguide propagation is extended to the continental shoulder or shallow water environment. By the image source method, the acoustical propagation solution is in conjunction with an extension of reflection analysis of spherical wave filed from a planar interface. Multiple reflections at the boundaries are taken as the originating from an image source depended on the surface and bottom positions. Analytical expression of acoustical pressure here is coupled with the Bessel function expansion in complex form. Two range-dependent cases, such as the along the slope (two dimension) and cross the slope (three dimension), are tested by the MPI and OpenMP parallelization and performance optimization. The multi-core platform of "Knights Landing" or KNL and many-core platform of "Tianhe-2" are applied to the utilization. The performance gain observed in using OpenMP of the FORTRAN code on high performance computing facilities is demonstrated.

Keywords: wedge, underwater acoustic propagation, MPI, OpenMP, Tianhe-2, KNL

1. INTRODUCTION

Underwater acoustic propagation is one of the basic contents in computational ocean acoustics [1]. Early studies mainly focused on the two-dimensional problem for the sake of limitation by the ocean environment data and computing ability. However, the underwater acoustic effects such as interface reflection greatly influence the propagation in a real complicated environment of ocean. In the process of solving the three-dimensional underwater acoustic field, some key difficulties are demonstrated as the high computational complexity and long time consuming, which limits its application in the matched field location, geoacoustic property inversion and array performance assessment for the calculating speed requirement [2]. With the rapid development of computer hardware and parallel optimization technology, it is one of the effective methods to propose high-efficiency and large-scale parallel algorithm of three-dimensional underwater acoustic propagation based on the latest high-performance platforms.

The three-dimensional acoustic propagation in a penetrable wedge is a theoretical model extracted from the shallow continental shelf and slope oceans [3]. An analytical solution of the sound field in a penetrable wedge with a stratified fluid or elastic basement was proposed by Dean and Buckingham [4], in which the surface and bottom reflections are explored by the image source method. Luo et al presented a generalized coupled-mode formulation was presented to calculate the wedge acoustic field by applying direct global matrix approach to obtain the modal expansion coefficients [5]. By using a square-root Helmholtz operator splitting algorithm, Ying et al proposed an alternating direction implicit three-dimensional fluid parabolic equation solution method with enhanced accuracy for the wedge problem [6]. The adiabatic mode parabolic equations were also used to approximate the solution of the three-dimensional Helmholtz equation by modal decomposition of the acoustic pressure field, in which the mode amplitudes satisfy parabolic equations that admit analytical solutions in the special case of the three-dimensional wedge [7]. Tang et al obtained the characteristics of horizontal refraction in the wedge-shaped ocean and released the MATLAB

* Correspondence: yxwang@nudt.edu.cn

code on the website of Ocean Acoustics Library [8]. Present work is aimed at the parallel implementation of three-dimensional acoustic field in a wedge waveguide after the transformation Tang's code to the FORTRAN version and performance test on the "Tianhe-2" and KNL platforms. It is expected to support the benchmark of three-dimensional range-dependent propagation problem from the perspective of computational speed.

2. BASIC MATHEMATICL PROBLEM

2.1 Reflection of Plane Waves

If the interface between two media is untitled as Figure 1, the spherical wave field is decomposed into a linear superposition of plane waves. For the sake of boundary reflection, these plane waves are only modified with amplitude, phase and direction of propagation. The reflection coefficient V on the interface is introduced to account for the quantitative change of plane wave properties. In the local Cartesian coordinate system of image source, $\vec{\mathbf{e}}$ is a unit vector normal to the interface. The wave-number vector $\vec{\kappa}$ and $\vec{\mathbf{e}}$ are here intersected at the incidence angle φ, which can be described as below.

$$cos\,\varphi = \frac{\vec{\mathbf{k}}\cdot\vec{\mathbf{e}}}{k} \tag{1}$$

In frequency domain, the spherical wave field at the receiver point is the contribution of homogeneous and inhomogeneous plane waves. For the former plane wave, the incidence angle φ is real from 0 to $\pi/2$. For the latter one, φ is varying form $\pi/2$ to $\pi/2 - i_\infty$ shown in Figure 2. Taken into account of plane-wave reflection, the coefficient V can be demonstrated as following.

$$V(\varphi) = \frac{(\rho_2/\rho_1)\gamma_1 - \gamma_2}{(\rho_2/\rho_1)\gamma_1 + \gamma_2} \tag{2}$$

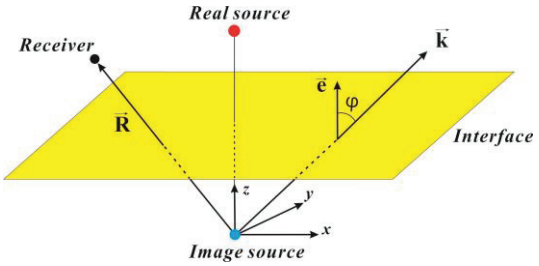

Figure 1 – Image source for untitled interface

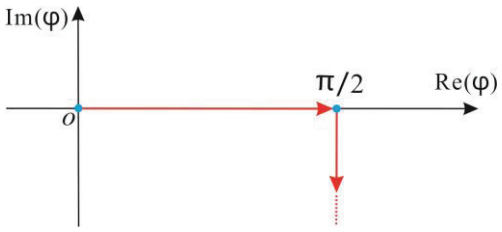

Figure 2 – Range value of φ for untitled interface

For the formula above, γ_1 and γ_2 are the magnitudes of the wave-number vector normal to the media interface in the upper and lower fluids respectively, whose expressions are responding to that

$$\gamma_1 = \frac{\omega}{c_1} cos\,\varphi, \qquad \gamma_2 = \frac{\omega}{c_2}\sqrt{1 - \left(\frac{c_2}{c_1}\right)^2 (1 - cos^2\,\varphi)} \tag{3}$$

where ρ_1 and $\rho_2$are the density values in the upper and lower fluids respectively, c_1 and $c_2$are the sound speeds in the upper and lower fluids respectively and ω is angular frequency for the harmonic point source.

2.2 Image Source for an Inclined Interface

In the wedge-like waveguide problem, there is an angle $\Theta$for the interface between two media, which can be drawn as the inclined case as Figure 3. In order to decompose the plane waves, it is necessary to apply the spherical polar coordinate system for the spherical wave field. Then the wave-number vector $\vec{\kappa}$ and coordinates (x_r, y_r, z_r) at receiver point can be transformed into the spherical polar forms.

$$k_x = k\,sin\,\theta\,cos\,\phi,\ k_y = k\,sin\,\theta\,sin\,\phi,\ k_z = k\,cos\,\theta \tag{4a}$$

$$x_r = R\,sin\,\zeta\,cos\,\xi,\ y_r = R\,sin\,\zeta\,sin\,\xi,\ z_r = R\,cos\,\zeta \tag{4b}$$

where θ or ζ is the angle between $\vec{\kappa}$ or $\vec{\mathbf{R}}$ and the oz axis and ϕ or ξ is the angle between the projection of $\vec{\kappa}$ or $\vec{\mathbf{R}}$ onto the xoy plane and the ox axis.

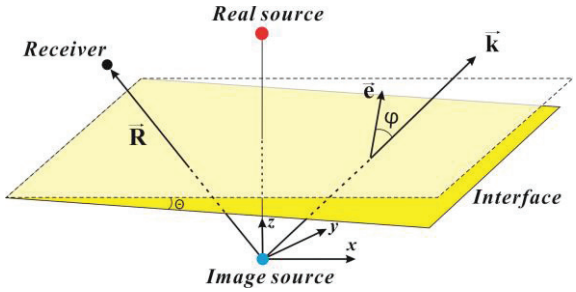

Figure 3 – Image source for inclined interface

By the coordinate transformation and variables separating, the mathematical representation of reflected acoustical field at the receiver point can then be written in the following formula.

$$p_r = \frac{ik}{2\pi}\int_0^{\pi/2-i\infty} e^{i\Omega_z(\theta)}\, sin\,\theta \times \int_0^{2\pi} V(\varphi) e^{i\Omega(\theta)\, cos(\phi-\xi)} d\phi d\theta \tag{5}$$

where $\Omega_z(\theta) = kR\, cos\,\theta\, cos\,\zeta$ and $\Omega(\theta) = kR\, sin\,\theta\, sin\,\zeta$ are derived from the dot product of $\vec{\kappa}$ and $\vec{\mathbf{R}}$. And the incidence angle φ is then expressed as the result of spherical components.

$$cos\,\varphi = sin\,\theta\, sin\,\Theta\, cos\,\phi + cos\,\theta\, cos\,\Theta \tag{6}$$

Here φ is the function of both θ and ϕ, which adds the integral difficulty of formula (5). It is well known that the integration of exponential term can be expanded in a Bessel function series. In the assumption of isotropic media, the reflected acoustical pressure can be simplified as below in the chosen coordinate system.

$$p_r = \frac{ik}{2\pi}\int_0^{\pi/2-i\infty} e^{i\Omega_z(\theta)}\, sin\,\theta \left(\frac{a_0 J_0(\Omega)}{2} + \sum_{\nu=1}^{\infty}(-1)^{\nu} a_{2\nu} J_{2\nu}(\Omega) + i\sum_{\nu=0}^{\infty}(-1)^{\nu} a_{2\nu+1} J_{2\nu+1}(\Omega)\right) d\theta \tag{7}$$

$$a_\nu = 2\, cos(\nu\xi)\int_0^{\pi} V(\varphi)\, cos(\nu\phi) d\phi \tag{8}$$

where J_0, $J_{2\nu}$and $J_{2\nu+1}$ are the first-kind Bessel functions of zero order, 2ν order and $(2\nu+1)$ order respectively and a_ν is the Fourier coefficient.

2.3 Acoustic Field in a Three-dimensional Wedge

The geometry of a wedge-like waveguide in three-dimension acoustical problem is shown as Figure 4. The angle of wedge apex is defined as Θwith the sea surface and bottom. A harmonic point source is placed in the three-dimension acoustical filed. In an orthogonal coordinate system, the origin O is fixed at the wedge apex, the positive OX axis is toward the wedge volume, the positive OZ axis is pointing downward and OY axis is along the wedge slope. Present work is aimed at the numerical calculation of acoustical propagation at receiver points in the three-dimension wedge-like waveguide.

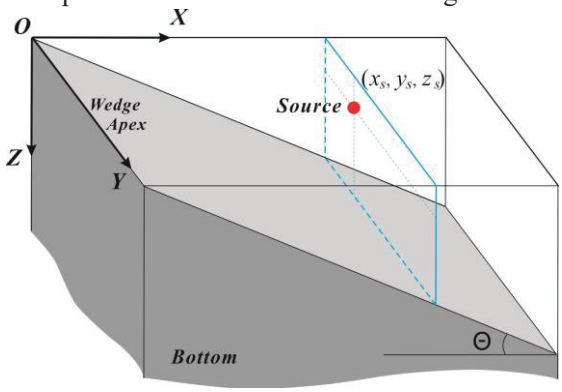

Figure 4 – Geometry of a wedge-like waveguide

Each reflection on both the surface and bottom boundaries raises the number of image source, which is located on the circle centered at the wedge apex. There are totally four kinds of image sources at specific reflection number n_b from the bottom boundary. In order to identify the image source uniquely, a parameter l is adopted with values of $(-2,-1,1,2)$. Whether the first reflection occurred at the surface or bottom is related to n_s, which is the number from the surface reflections. In the case of $l<0$, the image

source is below the bottom. For $l > 0$, the image source is above the bottom. The angle between a line passing through the source and wedge apex is defined as $\alpha_s = \Theta - tan^{-1}(z_s/x_s)$. If both the source location and wedge angle are specific, the angle of image source can be denoted as Φ_{nl}, which is taken the interface-reflection effect into account.

$$\Phi_{nl} = \begin{cases} -\alpha_s + 2\Theta(n_b + 1), & l = 2 \\ \alpha_s + 2\Theta n_b, & l = 1 \\ \alpha_s - 2\Theta n_b, & l = -1 \\ -\alpha_s - 2\Theta(n_b - 1), & l = -2 \end{cases} \tag{9}$$

The geometry of the image source in acoustic field is shown in Figure 5. For discrete receiver points in the space, the complex pressure of acoustic field can be obtained by the double integration as formula (10). If only the actual source is taken into account, the acoustic pressure at receiver point is related to the direct wave. However, the reflection of plane wave on the surface or bottom interface exerts significant effect on the acoustic field. For certain bottom reflection, more exact pressure should be the superposition by four kinds of image source. All the image sources are distributed on the arc such as Figure5. The quantitative value of acoustic field by a large enough numbern_b is less marked with the increase of bottom reflection, which hints that the acoustic pressure is convergent in the computational field.

$$p(x_r, y_r, z_r) = \sum_{n_b=0}^{n_{max}} \sum_l p_r(\vec{\mathbf{R}}, \Phi_{nl}) \tag{10}$$

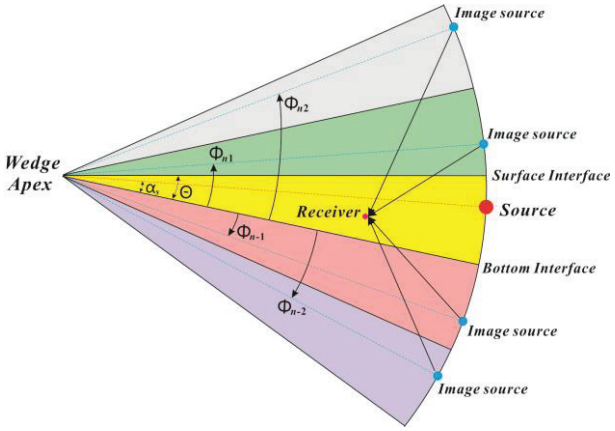

Figure 5 – Images of the source in acoustic field

3. DESIGN OF PARALLEL STRATEGY

3.1 Analysis of Computational Flow

Computational flow of the acoustic field by image source method is illustrated in Figure 6. Firstly, three-type parameters involving the actual source, receivers and environment are input. For actual source, it is necessary to obtain the frequency and coordinates in space. The exact position of receiver points should be also specific. Parameters of the environment are inclusive of the angle of wedge apex, sound speed in water and bottom.

Three loops are included in the whole framework. The number of bottom reflection$n_b$is related to the outer loop, which initiates the calculation or update of coefficient V for plane-wave reflection as part one. For the reason that specific image source is corresponding to the angle Φ_{nl}, the middle loop is related to the different kind of image source. If the interface is inclined, the Cartesian coordinates of actual source or image source and receiver points are then transformed into the cylinder ones. The output of coordinate transformation is then input to calculate the first-kind Bessel functions with multiple sequences denoted as part two. The contribution of actual source or image source to the acoustic field is described in a quantitative way by the production of Fourier coefficient and Bessel function in part three, where the reflection coefficients are needed from the part one of outer loop. Therefore, the computation of inner loop depends on the maximum number of Bessel sequence. Based on the superposition principle in numerical integration, the acoustic pressure is obtained by the Simpson integration for integral variableθ, which is marked as part four. If the difference between the former pressure at $(n_{max} - 1)$ and present one at n_{max} is small enough, the numerical results can be considered to be convergent and the whole computation is

then ended. From the view of computational complexity, the four parts mentioned above are very time-consuming.

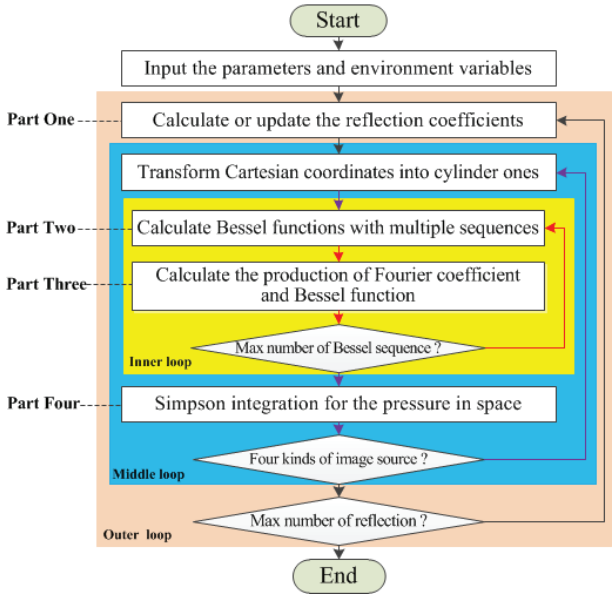

Figure 6 – Computational flow of the acoustic field by image source method

3.2 Task-level Decomposition

From the analysis of computational flow above, the acoustic pressure is solved by iteration related to the number of reflection, which determines that the outer loop can't be parallel implemented. Additionally, the reflection coefficient is relevant between the part one and part three. A feasible parallel solution may be mined for the fusion of middle and inner loops, in which the degree of parallelism is only the production between the maximum number of Bessel sequence and four kinds of image source. Such parallel implementation is limited to the high scalability.

The task-level decomposition in coarse granularity is here explored from the receiver points illustrated in Figure 7. In the condition of specific parameters for the actual source and environment, the calculation of acoustic pressure at each receiver point is absolutely independent. Therefore, the space of receivers can be divided into many subspaces in three dimensions and each subspace is then mapping to the specific computational task. This parallel implementation can be easily decomposed in the task level and extended to many CPU cores by the MPI model.

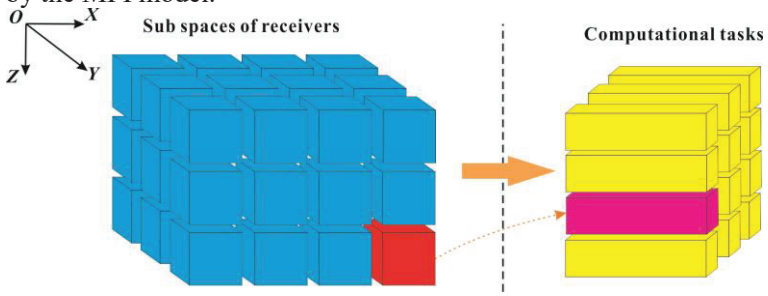

Figure 7 – Mapping from the subspaces to the computational tasks

The calculation of large matrix in some parts is especially compute-intensive, which may be suitable for the parallel implementation of OpenMP model. With the part one as example, pseudo code by the OpenMP parallel is illustrated in Figure 8. The dimension of reflection coefficient matrix is $\theta \times \phi$, which are corresponding to the integral variables in formula (7). For the sake of computational accuracy, the discrete number of θ or ϕ is generally set in the thousands. From the formulas (3) and (6), the variable φ is the function of θ and ϕ and each element in the reflection coefficient matrix is relatively independent, which is applicable to the task decomposition in different threads. During the program execution, each subtask is mapping to the computation of specific thread according to the set of OpenMP environment variable.

```
!$omp parallel &
!$omp & default(shared) &
!$omp & private( iph, ith, cos_phi_b, gam1, gam2)
!$omp do collapse(2)
 do iph = 1, nph                                                    % nph is the discrete number of ϕ
    do ith = 1, nth                                                 % nth is the discrete number of θ
       cos_phi_b = sin(theta_b)×sin(theta(ith))×cos( phi(iph))+cos(theta_b)×cos( theta(ith))   % formula (6)
       gam1 = k×cos_phi_b
       gam2 = k×sqrt( (c1/c2)^2-1.0 + cos_phi_b^2 )                 % formula (3)
       BotRefl = (rho2_rho×gam1-gam2)/(rho2_rho1×gam1+gam2)         % formula (2)
       Vtotal(ith, iph) = Vtotal(ith, iph)×BotRefl                  % update V
    enddo
 enddo
!$omp end do
!$omp end parallel
```

Figure 8 – Pseudo code of the OpenMP implementation for reflection coefficient

4. PERFORMANCE OF PARALLEL OPTIMIZATION

4.1 Platforms and Cases

Two types of computer platforms are considered in present work. They are the many-core platform of "Tianhe-2" and multi-core platform of Intel Xeon Phi 7250 (formerly Knights Landing, KNL). Super computer "Tianhe-2" is typical cluster structure, whose computing nodes are connected by high-speed internet and can communicate with each other. It is configured with the tens of thousands of Ivy Bridge processor and Xeon Phi coprocessor. This type of test platform was ranked as the fastest supercomputer in Top 500 from 2013 to 2016 [8]. KNL is the second generation with Many Integrated Core architecture, which is specifically designed for highly parallel workloads by Intel [9]. The working mode of KNL may be used as the master processor or a coprocessor whose peak performance per node can reach 3.0T FLOPS with double precision. KNL-7250 is advantageous of the optimal performance to power ratio between the four products launched by Intel in 2016. Table 1 lists the hardware and software configurations of above two platforms at one node.

Table 1 – Configurations of the test platforms at one node

Items	Tianhe-2	KNL
CPU type	Intel Xeon E5-2692 v2	Intel Xeon Phi 7250
CPU cores	24	68
CPU frequency	2.2 GHz	1.4GHz
Main memory	64 GB	16 GB
Operating system	Red Hat 6.5	Red Hat 4.8

The test cases of three-dimensional acoustic filed in a penetrable wedge include two conditions of the along-slope and cross-slope propagations at certain water depth. That is to say, the first case is for the receiver points on the OXZ plane and the second one is parallel to the OYZ plane in Figure 4. Some identical settings in both cases are inclusive of source frequency$f = 25\text{Hz}$, wedge angle $\Theta = 2.8624°$, sound speed in water $c_1 = 1500\text{m/s}$, sound speed in bottom $c_2 = 1700\text{m/s}$, water density $\rho_1 = 1.0\text{g/cm}^3$, bottom density $\rho_2 = 1.5\text{g/cm}^3$ and bottom attenuation $0.5\text{dB}/\lambda$. Other parameter settings are all listed in Table 2.

Table 2 – Settings of some parameters in the two test cases

Parameters	First Case	Second Case
Receiver position	$(x_r,\ 0,\ 30)$	$(4000,\ y_r,\ 30)$
Discrete number of receiver points	512	512
Source position	$(4000,\ 0,\ 100)$	$(4000,\ 0,\ 100)$
Discrete number for integral θ	7002	7002
Discrete number for integral φ	1001	1001
Maximum number of bottom reflection	9	30
Sequence number of first-kind Bessel function	2	50
Number of image source	38	122

4.2 Parallelization of Sequential Code

It is very important to parallelize sequential code for that the code must be operated in sequence in the parallel zone, single process or single thread. In order to compare the performance by different compiler and its options, several schedules are explored for the first case of wedge acoustic field on Tianhe-2 and KNL, whose results are illustrated in Figure 9. The high-level optimization of compiler is inclusive of –O3 and –O2 and the low-level optimization is for –O1 and –O0. The larger value of –O means higher parallelization. The option of –funroll-all-loops is loop unrolling, in which the compiler unrolls the loops to reduce the number of branches. Test results show that the consuming time on Tianhe-2 is rather less than that on KNL. The parallel performance is better if the compiler options of –O3 and –funroll-all-loops are both combined for the ifort than gcc.

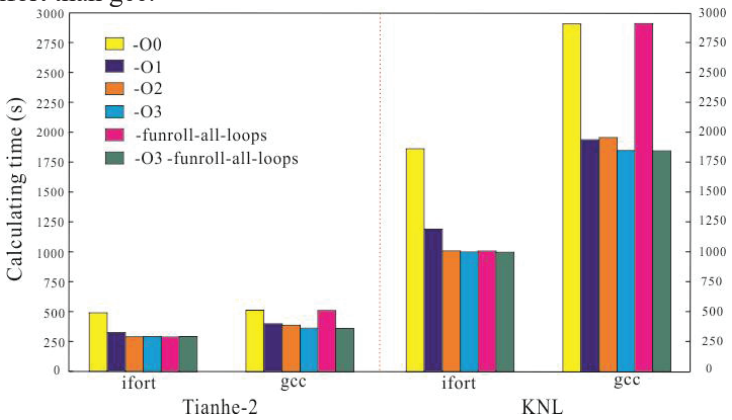

Figure 9 – Parallelization of sequential code by different compiler and options

4.3 Multi-thread Parallelization

Each node of KNL has 68 CPU(s) which can launch four threads simultaneously. For the first and second cases, multi-thread parallelization is implemented on the KNL platform, whose results are shown in Figure 10. If the thread number increases to 64, the speed up of performance is excellent. However, the parallelization is not good if the thread number is larger than 64. At these conditions, the multi-thread parallelization is up to the load limit of KNL, which is corresponding to the half-full-load status. However, the maximum number of threads is 272 for KNL in physical.

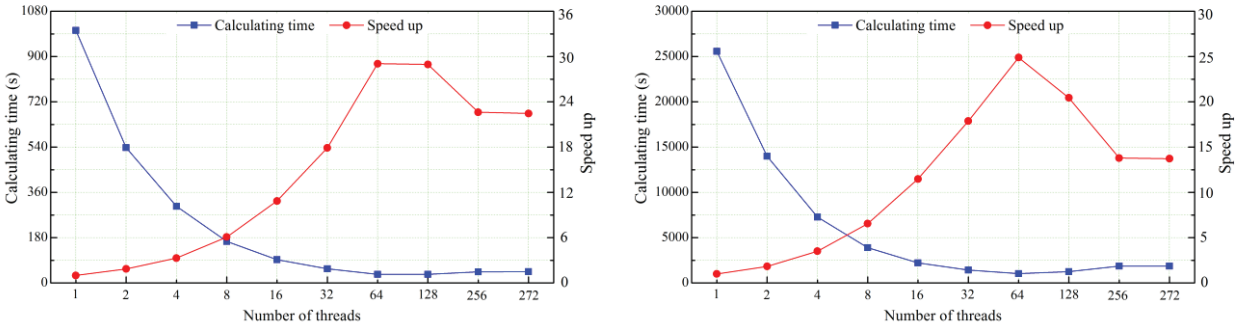

(a) First case (b) Second case

Figure 10 – Multi-thread parallelization on KNL platform

4.4 Hybrid MPI/OpenMP Parallelization

The performance test of hybrid MPI/OpenMP is also explored for the two cases. On the Tianhe-2 platform, different combination is configured for the 1×24, 2×12, 4×6, and 8×3, where the former number is corresponding to the processor and the latter one is to thread. From the test results in Figure 11, the performance of large thread number is better than that of processor number. Additionally, the calculating task of part three is very significant for the second case. By the hybrid MPI/OpenMP test, it can improve the performance by the proper combination of process and thread numbers.

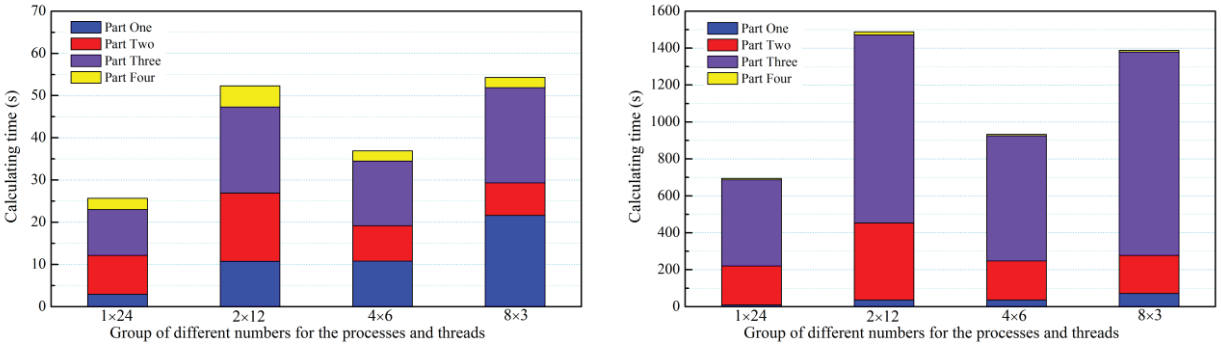

(a) First case (b) Second case

Figure 11 – Hybrid MPI/OpenMP parallelization on Tianhe-2 platform

5. CONCLUSIONS

For the three-dimensional acoustic field computation in a penetrable wedge by image source method, the parallel model by MPI and OpenMP is proposed in present work. The time-consuming and speed-up performances of sequential parallel, multi thread and hybrid MPI/OpenMP parallels are also tested on the Tianhe-2 and KNL. Some results demonstrate the good acceleration and scalability for further exploration.

ACKNOWLEDGEMENTS

Present work received financial support from the National Natural Science Foundation of China (No.51709267, No.61702531, No.61379056, No.61502516), National Key R & D Program of China (No.2016YFC1401800), Natural Science Foundation of Hunan Province, China (No. 2017JJ2305) and the Scientific Research Project of NUDT (No.ZK17-03-31, No.ZK16-03-31, No.ZK16-03-46).

REFERENCES

1. Jensen F B, Kuperman W A, Porter M B, et al. Computational Ocean Acoustics (Second Edition). Springer New York Dordrecht Heidelberg London, 2011.
2. Xu Min, Wang Yongxian, Anthony T C, Yue Hao. Parallelization and performance optimization of calculation in three-dimensional underwater acoustic propagation on modern many-core processor. IEEE International Conference on Signal Processing, Communications and Computing, 2018.
3. Kevin D H, Richard L C, James J M. Comparison of hybrid three-dimensional modeling with measurements on the continental shelf. Journal of the Acoustical Society of America, 2012. p. 1680-1688.
4. Deane G B, Buckingham M J. An analysis of the three-dimensional sound field in a penetrable wedge with a stratified fluid or elastic basement. Journal of Acoustical Society of America, 1993. p. 1319-1328.
5. Luo Wenyu, Yang Chunmei, Zhang Renhe. Generalized coupled-mode formulation for sound propagation in range-dependent waveguides. Chinese Physics Letters, 2012. p. 14302.
6. Ying Tsong Lin, Jon M Collis, Timothy F Duda. A three-dimensional parabolic equation model of sound propagation using higher-order operator splitting and Pade approximants. Journal of the Acoustical Society of America, 2012.p. 364-370.
7. Pavel S Perov, Frederic Sturm. An explicit analytical solution for sound propagation in a three-dimensional penetrable wedge with small apex angle. Journal of the Acoustical Society of America, 2016.p. 1343-1352.
8. Tang Jun, Piao Shengchun, Yang Xianpeng, Zhang Minghui. An analysis of horizontal refraction in the problem of sound propagation in wedge-shaped oceans. International Conference of Oceans, 2017.
9. Tianhe-2 championed global Top500 for sixth time. Sino Cast Daily Computers & Electronics Beat, 2015.
10. Jim Jeffers, James Reinders. Intel® Xeon Phi™ Coprocessors High-Performance Programming Knights Landing Edition. San Francisco: Margan Kaufmann, 2016.